# Using MRI data to compute a hand kinematic model

Patrick van der Smagt and Georg Stillfried

**Abstract** Even though there are many existing computational models of the kinematics of the human hand, none of them has the required precision sufficient to allow for rebuilding a model of the human hand. Embedded in a larger project in building a robotic arm mimicking the dynamics and kinematics of the human hand and arm, our goal is to obtain a detailed description of the kinematics of a human hand. The model is obtained from MR recordings of the bones of the hand, in a large number of different poses. The kinematic description should take all possible active, muscle-driven finger movements into account, including the complexity of the finger joints. The result of this model will be used in a simulation of the human hand, as well as a basis for reconstructing the hand as a robotic device.

## 1 Introduction

The human hand, in combination with the arm, is one of the utmost examples of highly intricate biomechanical structures, in which evolutionary optimality can clearly be distinguished. Optimised for both power and precision grasp, its structure with a thumb opposing four fingers is perfectly suited to solve every kind of daily task, be it precise grasping and handling or heavy duty lifting and grasping. As Kapandji [8] clearly shows, various important factors of the hand allow for this unmatched diversity in tasks. Not taking the sensing aspect into account, these include

- the dexterity of the thumb, having 5 (following [8]) or 4 [1] degrees of freedom, allowing it to oppone any of the four fingers;
- the rotation of the finger tips of the index, middle, ring, and little fingers towards the thumb, so as to optimise opposition with the thumb.

Patrick van der Smagt and Georg Stillfried
Institute of Robotics and Mechatronics, German Aerospace Center (DLR Oberpfaffenhofen), P.O. Box 1116, 82230 Wessling, e-mail: smagt@dlr.de

On the other hand, even the most advanced robotic grippers such as the UB Hand [2], Robonaut Hand [11], Karlsruhe Hand [9], DLR Hand [3] do not take this fine opposition into account. Rather, robotic hands are constructed to mimic the look and up to four degrees of freedom per finger, neglecting the important role of the thumb and of the movement of the fingers. Consequently, robotic hands are not nearly as dextrous as human hands, even though they have come a long way since the ancient robotic pick-and-place grippers from the 80s and early 90s.

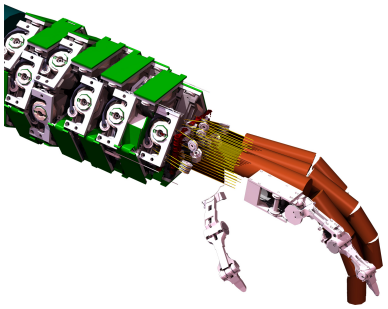

**Fig. 1** CAD design of the planned integrated DLR hand-arm system.

At the Institute of Robotics and Mechatronics of the German Aerospace Center (DLR Oberpfaffenhofen), an effort is underway to construct a robotic system mimicking the kinematics and dynamics of the human hand and arm as closely as possible with modern mechatronic approaches. This system, depicted in Figure 1, is based on a co-contractive (antagonistic) drive system with joint structures as close to the biological counterpart as possible [6]. In order to construct this system, detailed knowledge of the human hand and arm is required. Much of these data can be obtained by studying corpses; the larger part of these information is available in medical literature. This is not true, however, for the kinematics of the human hand. Even though detailed medical analytical books on the human hand exist, foremost those by Kapandji, these publications focus on such information needed to repair injuries. Computational models, like their robotic realisations, ignore all less obvious effects and treat the PIP and DIP joints as simple hinge joints with axes perpendicular to the links.

We plan to radically change this situation. Using modern imaging techniques based on magnetic resonance imaging (MRI), we recorded a vast number of images of the bones of the human hand; in our case, recordings of a healthy 29-year old female hand was used. Using automatic and manual segmentation techniques and novel localisation methods, we used the resulting data to create a detailed, kinematic model of the human hand.

This paper describes our solution to this problem. Section 2 explains some of the intricacies of the human hand. Section 3 describes our recording methods, while section 4 describes our segmentation and localisation approaches. The resulting model is described in section 5, followed by a conclusion in section 6.

## 2 The human hand

In our design of an anthropomorphic hand our goal is to closely copy the *properties* of the hand rather than its intrinsic structure. The solutions found in biology must be transferred to technical components and evaluated before they can actually be used. Therefore our investigation is not targeted at disentangling the structure of the human hand, but rather unravel how it works.

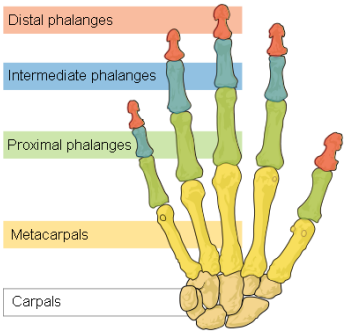


**Fig. 2** Nomenclature of the bones in the human hand. From [12].

The human hand consists of a palm with metacarpal bones and finger bones, the proximal, medial and distal phalanxes. The index, middle and ring finger are similar in their structure and configuration, whereas the thumb and little finger differ considerably; the latter has a bone structure similar to the middle fingers but its tendons, ligaments and muscles resemble those of the thumb.

The human hand uses mainly three kinds of joints, which, according to Kapandji [8], can be divided into 1-DoF and 2-DoF joints. Benninghoff [1] also mentions 3-DoF joints in the thumb. The 1-DoF joints in the hand all are hinge joints; the 2-DoF joints can be divided into two types. The metacarpal joint of the thumb is a saddle joint but with non-orthonormal axes and can be described by the saddle of a scoliotic horse [10]. In contrast, the metacarpal joints of the fingers are condyloid. The main difference between saddle and condyloid joints is that condyloid joints have (roughly) intersecting axes which saddle joints do not have. For the thumb, the axes of the metacarpal are non-orthogonal screw.

The special structure of the joints leads to an important effect, necessary for the opposition of the fingers with the thumb, bringing together the pulp of the thumb and the opposing finger (see Figure 3). To obtain coincidence of the planes, five degrees of freedom are used [8]: three for the thumb, one for flexing the (in this case) index finger, and one for rotating the pulp of the index finger towards the thumb. It is this latter rotation which is essential for grasping but not quantified or modelled in any existing robotic approach.

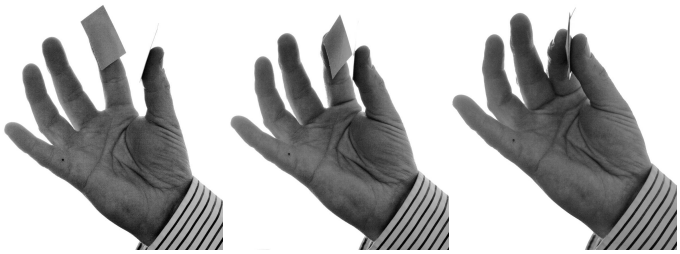

**Fig. 3** Opposition of the index finger and thumb of the human hand. The two faces, parallel to the finger tip, can only meet due to the rotation of the most distal phalanx of the index finger during flexion.

## 3 Data recording

Recording the kinematic movement of the human hand is not an easy thing to do. It must be taken into account that only *in vivo* recordings can be used to measure the effects described; after all, the behaviour of the soft tissue, tendons, and muscular structure greatly influence the kinematics of the *active* hand.

All known methods have sofar concentrated on observing the hand from the outside. As an example, Fioretti [4] used a camera system to observe the rotation of the index finger, in order to obtain data on the MCP bone. Other approaches have concentrated on visually measuring the joint angle of the fingers, or even used inaccurate devices such as DataGloves [5]. All of these methods, however, suffer from the problem that they do not use fixed reference points on the hand, but rather use a specific point on the skin as a stable reference point.

Even though the whole skin in itself, and especially the part of the finger tips with which the grasp is performed, is a key element in grasping, choosing any point on the skin gives a point of reference which changes during hand motion, and cannot be considered a stable point. All of the methods using markers on the hand are therefore rather imprecise; rather than measuring the motion of the whole finger, they measure the motion of one or more points on the skin, being subject to both active and passive influences.

In order to obtain a static reference point, we therefore decided to rather investigate the movement of the *bones* in the hand, rather than any soft tissue reference point.

In order to simplify the recording of the hand movement, and due to the fact that we need *in vivo* measurements, invasive methods to use the bones as markers were not considered. Rather we decided to use modern imaging methods to locate the hand and finger bones at the awake adult. Considering the high resolution that is required for these measurements, two viable approaches exist: (1) CT imaging and (2) MR imaging.

1. **CT imaging** (Computed Tomography) is a medical imaging method employing tomography where digital geometry processing is used to generate a three-

dimensional image from a large number of two-dimensional X-ray images taken around a single axis of rotation. The nature of X-ray imaging makes it very well suited for bone imaging, and high-resolution 3D images can be obtained in a matter of seconds or minutes. However, CT relies on ionizing radiation, which is known to cause cancer or perhaps even cause leukemia in very high radiation doses. Therefore, we decided to exclude CT from our investigations.

2. **MR imaging** (Magnetic Resonance) has much greater soft tissue contrast than CT, without using ionizing radiation. The scanner creates a powerful magnetic field which aligns the magnetization of hydrogen atoms in the body. This causes the hydrogen atoms to emit a weak radio signal which is detected by the scanner and used to create a 3D image. Even though MR imaging is slower and results into lower resolution imaging, there are no health risks involved.

After several rounds of setting the correct parameters for the MR scanner we used in our experiments, we ended up with doing 4-minute steady 3D scans of the hand, with an isotropic resolution of $(0.76\text{mm})^3$, with an 8-bit resolution per voxel. Since we still considered this resolution to be too low, we then automatically interpolated the images, which then resulted in a resolution of $(0.38\text{mm})^3$ per voxel. In order to both record the full hand, and obtain enough detail in the end phalanxes, we used a 8-channel Philips-SENSE-8 head coil, leading to highly homogeneous signals. The data were recoreded with a 1.5T Philips Achieva scanner, using a balanced steady-state free precession (b-SSFP) sequence.

In total, approximately 100 images of the hand in various positions were recorded.

## 4 Finding the bones

After data recording, the bones in each of the images were manually segmented and separately stored using the 3D Dicom imaging tool Amira. This manual preprocessing step lead to a set of segmented bones, each one being represented by a set of grey voxel values with 3D coordinates (see Figure 4).

**Fig. 4** Segmenting the proximal phalanx of the little finger in Amira. (left) Automatic segmentation with manual correction in per slice; (middle) Corrected slice segmentation; (right) Segmented area mapped on the recording of the bone, resulting in an 8-bit representation of the bone.

As a first step, we needed to know the position and orienation of each bone in each MR image. We defined one of the recorded hand poses as the referece pose. (The recording shows a relaxed hand pose.) We defined the position and orientation of a bone in another image as the translation and rotation that is necessary to map the bones onto each other (See Figure 6). This motion was found using a visual localisation approach described in [7]. It works by drawing point triples from both images and comparing point triples with similar edge lengths. The motion that is suitable to make most of these triangle pairs congruent is considered the best estimation for the motion of the bone from one image to the next.

Initially, the results showed a very high uncertainty for the DIP joint of the index finger. It turned out that the distal phalanx of the index finger had often been estimated to lie rotated about 180 degrees around its centre-line, when compared to its actual orientation. The reason for this is its nearly symmetrical shape. In order to avoid this error we used a modified version the pose estimator that only allows rotation angles up to 120 degrees.

Another step to improve pose estimation was to take only points close to the surface of the bones. This increases the probability that triangle pairs with similar edge length lie at the same position of the bone. We took a higher percentage of points for the small bones, in order to account for their higher surface-to-volume ratio.

## 5 Building a model

We modeled the human hand as a set of five kinematic chains, one for each finger (See Figure 5). The chains lead from the basis of the index finger metacarpal, shown as a black sqare, to the respective fingertips, shown as black diamonds. The joints are represented by black balls. The MCP joints of the fingers and the CMC joint of the thumb are modelled as 2-DoF rotational joints with intersecting axes. The first axis of rotation is indicated as red arrow, the second axis as green arrow. The PIP and DIP joints and the thumb IP joint are modelled as 1-DoF rotational joints. Their axes of rotation are indicated by red arrows.

For each joint, three sets of parameters had to be calculated:

1. The positions of the centres of rotation (CoR),
2. the orientations of the axes of rotation (AoR),
3. the scope of the rotation angles.

The basis for the calculation of the above parameters is the relative motion of the distal bone of a joint with respect to the proximal bone[1].

For this purpose we consider the proximal bone of the joint as fixed and the distal one as varying. In order to calculate the relative motion between the reference

[1] *Proximal* denotes structures that are closer to the body, *distal* denotes structures that are father away from the body.

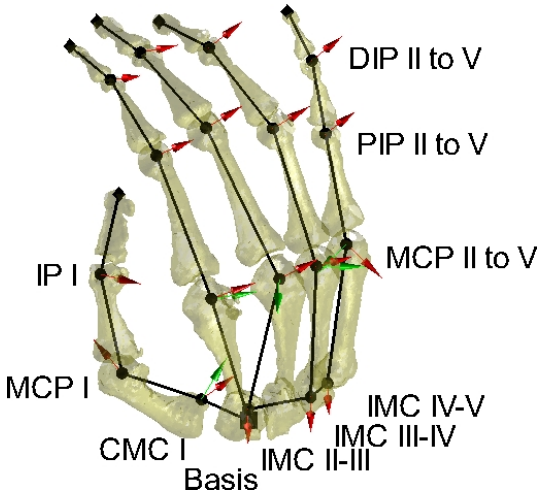


**Fig. 5** The hand model. The fingers are numbered from I for thumb to V for index finger.

image and another image, we translocate the bone pair of the other image so that the proximal bones coincide (see Figure 6 (left)).

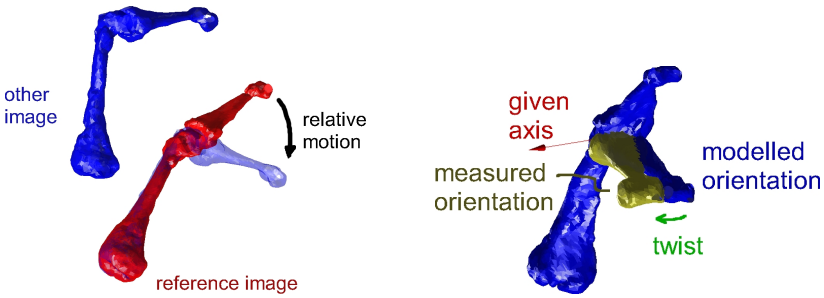


**Fig. 6** (left) Relative motion. (right) Twist as a measure of difference between orientations.

If we denote the pose estimations by the following homogenous transformation matrices, $\mathbf{T}_{\mathrm{P,ref}\to i}$ for the pose estimation of the proximal bone of image $i$ (with respect to its counterpart in the reference image) and $\mathbf{T}_{\mathrm{D,ref}\to i}$ for the pose estimation of the distal bone of image $i$, the relative motion $\mathbf{T}_{\mathrm{Rel},i}$ is computed by

$$\mathbf{T}_{\mathrm{Rel},i} = \mathbf{T}^{-1}_{\mathrm{P,ref}\to i}\,\mathbf{T}_{\mathrm{D,ref}\to \mathbf{i}} \tag{1}$$

We compute the positions of the joint centres of rotation (CoRs) and the orientations of the joint axes of rotation (AoRs) by way of numerical optimisations. For the CoRs we minimise the mean distance about which a point is deplaced by the

relative motions. This comes from the rationale that, in an ideal rotational joint, the CoR is at the same place before and after a movement of the joint.

For the AoRs, we minimise the mean twist between the modelled and measured orientations of the distal bone. The twist is defined as the rotation angle of an additional rotation that is needed to map the the modelled orientation on the measured one (see Figure 6 (right)). The optimisation of the AoR is in fact a nested optimization consisting of an inner and and outer optimization. The inner optimisation takes a given axis and finds the rotation angles that minimise the twist between the modelled and the the recorded orientations. The outer optimisation finds an axis orientation that results in the minimal *mean* twist.

The scope of the rotation angle is finally established by the minima and maxima of the inner optimisation rotation angles, that is, the rotation angles that move the bone closest to its extreme positions.

## *5.1 Results*

As results we present the positions of the centres of rotation, the orientations of the axes of rotation and the scope of the rotation angle. We also quantify the uncertainty of the results.

The results are given in a coordinate system fixed to the index finger metacarpal. The x-axis points towards the thumb (radial direction); the y-axis points toward the back of the hand (dorsal direction); and the z-axis points in longitudinal direction of the bone towards its distal end (See Figure 7). The unit is Millimetres.


**Fig. 7** The coordinate system in which the results are presented.

The positions of the CoRs and the orientations of the AoRs are shown in Table 1. The uncertainty of the position is given as the mean translational deplacement between the modelled and the measured positions. The uncertainty of the orientation is given as the mean twist between modelled and measured orientation.

The uncertainties are due to both the uncertainty of the pose estimation as well as to the discrepancy between the joint model and the real joint. The mean deplacement is small (about 1 mm) for most joints. From this we can conclude that it is appropriate to model the joints as purely rotational joints. An exception is the thumb CMC

joint, with a deplacement of 4.8 mm. The reason for this could either be a translational movement of the joint, or the fact that the actual axes of rotation do not intersect.

For the orientation, we consider twists up to 5 degrees acceptable. The joints with higher twist need further investigation.

Common robotic hands have joint axes orthogonal to the links. The last column of Table 1 shows the inclinations of the 1-DoF-joints. The inclination is the angle between an orthogonal axis and the axis we found in our optimisations. A significant inclination is found in the MCP I, the DIP III and the DIP V joint.

| joint | CoR | | | mean deplacement | AoR | | | mean twist (degrees) | inclination (degrees) |
|---|---|---|---|---|---|---|---|---|---|
| CMC Ia | 9.3 | -12.5 | 4.5 | 4.8 | -0.922 | -0.310 | -0.231 | | |
| CMC Ib | | “ | | | -0.831 | -0.264 | 0.491 | 4.9 | |
| MCP I | 31.1 | -11.7 | 36.7 | 0.8 | 0.140 | -0.970 | 0.198 | 9.0 | 18.0 distally |
| IP I | 25.9 | -22.2 | 72.8 | 1.1 | -0.554 | 0.818 | 0.150 | 7.8 | 2.7 proximally |
| MCP IIa | 0.0 | -0.0 | 64.4 | 0.8 | -0.979 | 0.017 | -0.204 | | |
| MCP IIb | | ” | | | -0.926 | 0.121 | -0.358 | 4.2 | |
| PIP II | -5.7 | -36.7 | 93.4 | 0.7 | -0.893 | -0.216 | -0.396 | 4.4 | 2.4 distally |
| DIP II | -5.4 | -64.1 | 102.3 | 1.6 | -0.686 | -0.238 | -0.688 | 6.8 | 0.0 |
| IMC II-III | -0.2 | 2.4 | 8.7 | 0.7 | 0.227 | 0.053 | -0.972 | 1.8 | |
| MCP IIIa | -21.8 | 2.6 | 60.5 | 0.7 | -0.939 | -0.196 | -0.280 | | |
| MCP IIIb | | “ | | | 0.470 | 0.869 | 0.157 | 2.8 | |
| PIP III | -22.8 | -34.9 | 96.4 | 0.8 | -0.935 | -0.241 | -0.259 | 4.8 | 2.7 distally |
| DIP III | -17.6 | -66.6 | 104.0 | 1.1 | -0.836 | -0.122 | -0.536 | 4.7 | 10.8 proximally |
| IMC III-IV | -19.9 | 4.1 | 1.4 | 0.6 | 0.227 | 0.053 | -0.972 | 3.0 | |
| MCP IVa | -35.3 | -2.0 | 51.2 | 1.2 | -0.801 | -0.207 | -0.562 | | |
| MCP IVb | | ” | | | -0.872 | 0.449 | -0.192 | 6.3 | |
| PIP IV | -40.6 | -25.3 | 93.0 | 0.7 | -0.937 | -0.240 | -0.253 | 4.7 | 2.1 proximally |
| DIP IV | -35.3 | -52.1 | 109.3 | 2.3 | -0.919 | -0.335 | -0.204 | 4.8 | 2.7 distally |
| IMC IV | -26.9 | 1.4 | 0.1 | 1.0 | 0.165 | -0.010 | -0.986 | 2.9 | |
| MCP Va | -48.7 | -11.3 | 41.3 | 0.8 | -0.317 | 0.780 | -0.538 | | |
| MCP Vb | | “ | | | 0.906 | 0.404 | 0.123 | 3.4 | |
| PIP V | -56.3 | -26.0 | 77.0 | 0.9 | -0.824 | -0.422 | -0.376 | 6.4 | 4.0 proximally |
| DIP V | -61.6 | -36.7 | 99.1 | 0.9 | -0.852 | -0.417 | -0.315 | 6.0 | 7.0 distally |

**Table 1** Results: Positions of the centres of rotation and orientations of the axes of rotation, with their respective uncertainties.

## 6 Conclusion

We have introduced a novel approach to setting up a detailed kinematic model of the human hand. The whole hand is modelled, with 1-DoF-joints for the IP, PIP and DIP joints and 2-DoF joints for the finger MCP and the thumb CMC joints. While most of the joints have axes nearly orthogonal to the logitudinal axis of the bone, the MCP I, the DIP III and the DIP V joint showed to have a significant inclination. Further investigation of the hand kinematics will be done using different types of joint models, for example 2-DoF joint with not intersecting axes.

**Acknowledgment.** This work has been partly funded by SENSOPAC (FP6-IST-028056).

**Abbreviations.** The following abbreviations have been used in this paper:

| | | | |
|---|---|---|---|
| AoR | axis of rotation | DoF | degrees of freedom |
| CMC | carpo-metacarpal joint | IMC | intermetacarpal joint |
| CoR | centre of rotation | MCP | metacarpo-phalangeal joint |
| CT | computed tomography | MR(I) | magnetic resonance (imaging) |
| DIP | distal interphalangeal joint | PIP | proximal interphalangeal joint |

## References

1. A. Benninghoff and D. Drenckhahn. *Anatomie. Makroskopische Anatomie, Histologie, Embryologie, Zellbiologie, Bd. 1*. Urban & Fischer at Elsevier, 2002.
2. L. Biagiotti, F. Lotti, C. Melchiorri, G. Palli, P. Tiezzi, and G. Vassura. Development of UB hand 3: Early results. In *2005 IEEE International Conference on Robotics and Automation*, 2005.
3. J. Butterfass, M. Fischer, and M. Grebenstein. Design and experiences with DLR hand II. In *Proceedings of the World Automation Congress*, 2004.
4. S. Fioretti. Three-dimensional in-vivo kinematic analysis of finger movement. In F. Schuind, K.N. An, W.P. Cooney III, and M. Garcia-Elias, editors, *Advances in the Biomechanics of the Hand and Wrist*, pages 363–375. Plenum Press, 1994.
5. M. Fischer, P. van der Smagt, and G. Hirzinger. Learning techniques in a dataglove based telemanipulation system for the DLR hand. In *Transactions of the IEEE International Conference on Robotics and Automation*, pages 1603–1608, 1998.
6. M. Grebenstein and P. van der Smagt. Antagonism for a highly anthropomorphic handarm system. *Advanced Robotics*, 22:39–55, 2008.
7. U. Hillenbrand. Consistent parameter clustering: definition and analysis. *Pattern Recognition Letters*, 28:1112–1122, 2007.
8. A. Kapandji. *The Physiology of the Joints*. Churchill Livingstone, 1998.
9. A. Kargov, T. Asfour, C. Pylatiuk, R. Oberle, H. Klosek, S. Schulz, K. Regenstein, G. Bretthauer, and R. Dillmann. Development of an anthropomorphic hand for a mobile assistive robot. In *9th International Conference on Rehabilitation Robotics*, pages 182–186, 2005.
10. K. Kuczynski. The thumb and the saddle. *Hand*, 7(2):120–122, 1975.
11. C. S. Lovchik and M. A. Diftler. The robonaut hand: a dexterous robot hand for space. In *Proceedings 1999 IEEE International Conference on Robotics and Automation*.
12. Wikipedia. Hand. http://en.wikipedia.org/wiki/Hand, 2008.